Siaud and Ulmer-Moll *EURASIP Journal on Wireless Communications and Networking* (2016) 2016:92
DOI 10.1186/s13638-016-0588-2

EURASIP Journal on Wireless Communications and Networking
a SpringerOpen Journal

RESEARCH Open Access

Green-oriented multi-techno link adaptation metrics for 5G heterogeneous networks

Isabelle Siaud[1,2*] and Anne-Marie Ulmer-Moll[2]

Abstract

Fifth generation (5G) technical requirements turned toward end-to-end capacity increase with limited latency and constant network power consumption involve dedicated research topics. Multiple radio access techniques are one of the most promising paradigm safeguarding throughput increase and seamless connectivity in heterogeneous networks. Link adaptation metrics are then required to achieve radio link selection and multiple interface management. Following mobile network capacity increase trends, link adaptation metrics focused on spectrum efficiency maximization are implicitly sought, involving high network power consumption. This paper presents a novel link adaptation metric turned toward a power efficient radio link selection which warrants QoS and performs a fair comparison between independent air interfaces in a multiple radio access technique context. A procedure is proposed to practically evaluate the metric upon each air interface, thanks to the introducion of new normalized propagation selectivity parameters with respect to system parameters allowing a unified characterization of the propagation link reliability, tuning up the metric decision. Performance and transmit power gains resulting from the metric application are appraised upon wireless hot spot extensions covering 5GHz and 60GHz Wi-Fi technologies and mm-wave ultra-wide-band transmissions.

Keywords: Energy efficiency, Link adaptation metric, Multiple interface management, Cooperative networks

1 Introduction

Fifth generation (5G) technical requirements [1] turned toward 1000 time end-to-end capacity increase with latency up to 1 ms and optimized network power consumption involve new research topics. Multiple radio access techniques (multi-RAT) deployed in heterogeneous networks (HetNets) is one of the most promising solutions to improve network capacity and ensure seamless connectivity with a high quality of service (QoS). Multi-RAT management processing [2] performed with power efficiency (PE) link adaptation techniques and scalable spectrum management will ensure seamless connectivity in a high multi-user context, limiting multi-user interference, and guarantying QoS along with radio coverage. Innovative power efficient cooperative networks justify matter of necessity to develop new link adaptation metrics.

The paper introduces and evaluates a novel link adaptation metric turned toward PE radio link selection intended for multi-RAT cooperative networks. The present work has been initiated in the ICT-FP7 METIS project inquiring into new physical (PHY) waveforms and multi-RAT architectures for 5G (https://www.metis2020.com/) [3, 4]. Embedded solutions adapted to mm-wave overlay networks are currently outperformed in the ICT-FP7 Europe-Japan MiWEBA project (http://www.miweba.eu/#Project). MiWEBA addresses mm-wave ultra-broadband phantom cells integrated in mobile cellular networks and backhauling scenarios [5–7]. Multi-RAT architectures are examined, regarding novel power-efficient link adaptation metrics enable to switch between RATs [2] and their integration into innovative control/user (C/U) plane splitting architectures [8–10] in accordance with the 3GPP wireless local area network/Long Term Evolution-Advanced (WLAN/LTE-A) carrier aggregation study item [11]. In the GreenTouch Consortium [12] and MiWEBA project

* Correspondence: isabelle.siaud@orange.com
[1]OLN/RNM/AWE/CREM department, Orange Labs Networks, Rennes, France
[2]OLN/RNM/RCS/W3A department, Orange Labs Networks, Rennes, France

[8], new C-plane information exchanges steer small cell activation for U-plane transmissions.

Link adaptation techniques strive for spectrum efficiency (SE) optimization following throughput increase target settings for embedded 5G networks [13, 14]. Holistic solutions combine adaptive modulation and coding (AMC) at the physical layer and hybrid automatic retransmission request (HARQ) at the medium access control layer to improve SE and link reliability [15]. Differentiated link adaptation processing [16] is tackled to perform a personalized user HARQ adaptation. 3GPP and Wi-Fi physical layer procedures [17, 18] embrace a SE link adaptation processing for multi-RAT offloading [13]. Trade-off between SE and energy-efficient link adaptation processing is undertaken on LTE-A, addressing dynamic and static power consumption of digital baseband processing at the PHY layer [19].

Section 2 exposes the SE link adaptation techniques focused on throughput maximization bound with received signal strength and AMC to select transmission modes (TMs) in HetNets. Section 3 details the novel PE link adaptation metric proposed in the paper, which is denoted the Green Link Budget (GLB) metric, and accounts for assessment methods for software implementation in multi-RAT architectures. Section 4 deals with the performance and transmit power gains resulting from the GLB metric application upon MiWEBA test cases [5] covering mm-wave ultra-wideband (UWB) transmissions [20] and Wi-Fi extensions for indoor and hot spots. Conclusions of this paper detail perspectives of this work currently carried out in the MiWEBA project.

2 A focus on spectrum-efficient link adaptation processing

Spectrum efficiency based link adaptation techniques follow throughput increase target settings for embedded heterogeneous networks and mobile data offloading. These techniques result from several AMC figures as cited in Section 1, usually applied on a single air interface able to operate in several radio frequency bands combined with access network discovery and selection function (ANDSF) to control offloading between 3GPP and non-3GPP access networks [21]. Hence, in a single air interface context, link adaptation metrics select the highest possible data rate mode associated to the largest modulation order in accordance with a measured received signal strength indicator (RSSI) related to a maximum block error rate (BLER) threshold and look-up tables (LUTs) giving the correspondence between an equivalent signal-to-noise ratio (SNR) and the modulation and coding scheme (MCS) [13–16, 18, 19, 22].

An illustration is done for the Long Term Evolution-Advanced (LTE-A) downlink (DL) transmissions following 3GPP technical specifications [17, 23] and literature issues [16, 18, 19, 22]. In LTE-A, the evolved node base station (E-Node-B) makes the decision of the selected MCS for DL transmissions, using proprietary algorithms and a channel quality indicator (CQI) feedback reported by the user equipment (UE) to the E-Node B. As shown on Fig. 1, the E-node B forwards dedicated pilots to the UE in order to estimate RSSI on the DL. The UE converts the RSSI into an energy-per-bit-to-noise-power-spectral-density ratio, Ec/N_0, and determines a CQI index such that it corresponds to the highest MCS allowing the UE to decode the transport block with error rate probability not exceeding 10 % [18, 22]. From the BLER-versus-SNR plot, the SNR value for acceptable 10 % BLER is taken for each CQI value ranging from 1 to 15. The UE converts it into a 4-bit CQI word and forwards it to the E-Node B upon a reverse link using the channel quality indicator channel (CQICH) which supports forward link packet data operations. The E-Node B converts the 4-bit CQI word into SNR and uses proper CQI-to-SNR mapping tables to select MCS and throughput for DL. The E-Node B takes the decision of the MCS for the DL transmission which is close as possible as the UE CQI feedback.

A UE with receiver of better quality may report better CQI and thus can receive downlink data with a higher MCS. The procedure is illustrated on the Fig. 1 giving referenced standards in the process. The correspondence between Ec/No, 4-bit CQI world, CQI index, and MCS parameters is compiled in the table using [18, 22] information. CQI-to-SNR mapping for the LTE-A is illustrated on Fig. 2. The left and right figures show that the CQI index hikes up with the modulation order M, data throughput and required SNR levels guarantying BLER targets.

An analytical expression is given in [19] to establish the relation between the SE, MCS, and power requirements upon DL LTE-A transmissions:

$$\begin{aligned} \mathrm{SE} &= \frac{1}{2}\frac{(1-\mathrm{BLER})R_c N_{\mathrm{cbps}} L}{10^{-3}} \\ M\cdot R_c &= 2^{N_{\mathrm{cbps}}} R_c = \frac{1}{2}\frac{10^{-3}}{(1-\mathrm{BLER})L}\cdot\left(1+\frac{\mathrm{EIRP}\cdot g_n}{BN_0}\right) \end{aligned} \quad (1)$$

R_c is the coding rate, N_{cbps} is the number of encoded bit per modulation constellation point, i.e., per subcarrier, and L is the number of subcarriers per resource block (RB) in the LTE-A subcarrier assignment. g_n is the average channel gain on RB, N_0 is the noise power spectral density, and B is the bandwidth per RB. EIRP is the emitted isotropic radiated power. Equation (1) shows that, for a fixed BLER, the SE is linearly increasing with the number of information bits per subcarrier given by R_c N_{cbps}. The modulation order M linearly builds up with a transmit EIRP expansion and an equivalent SNR derived from the average channel gain g_n in a RB.

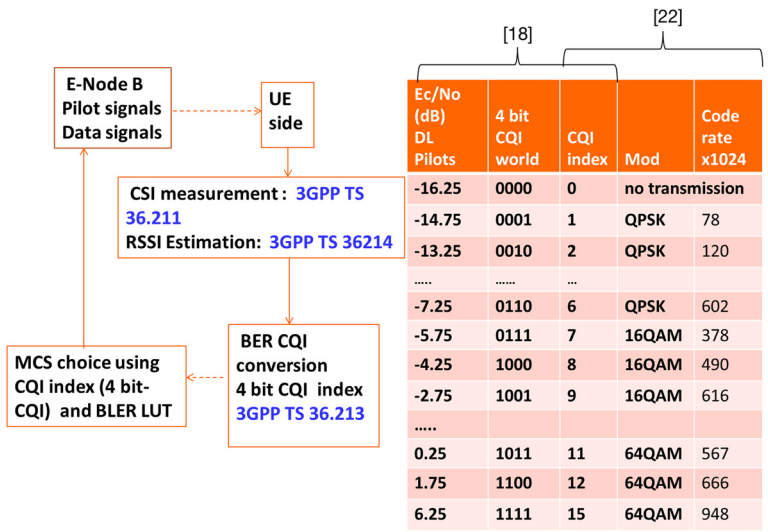

Ec/No (dB) DL Pilots	4 bit CQI world	CQI index	Mod	Code rate x1024
-16.25	0000	0	no transmission	
-14.75	0001	1	QPSK	78
-13.25	0010	2	QPSK	120
.....	.....	...		
-7.25	0110	6	QPSK	602
-5.75	0111	7	16QAM	378
-4.25	1000	8	16QAM	490
-2.75	1001	9	16QAM	616
.....				
0.25	1011	11	64QAM	567
1.75	1100	12	64QAM	666
6.25	1111	15	64QAM	948

Fig. 1 LTE-A AMC mechanism using CQI-to-MCS mapping

In IEEE802.11 technologies, RSSI is acquired during the preamble stage of receiving an 802.11 frame and the RSSI is adjusted accordingly to manufacturers with CQI index range set to 0 to 100.

The proposed link adaptation (LA) metric, exposed in the next section which is denoted the green link budget (GLB) metric, works with a targeted data throughput attached to the transported service and QoS, which may be delivered by several air interfaces embracing several MCS, variable bandwidths, and different types of baseband processing. The selection is steered toward a power efficient criterion which may exhibit variable SE levels.

3 The Green Link Budget metric model

The GLB metric, composed of two metrics α and β, is a multi-technology link adaptation (MT-LA) metric, which selects transmission modes (TMs) of various interfaces in targeting on a data throughput determined by the service to transport and a selection emphasizing transmission modes revealing lowest degradations at the PHY layer and the minimum propagation path-loss deduced from the received power measurements. TMs stand for baseband processing and radio frequency (RF) specifications at the PHY layer. In addition, the GLB metric performs a dynamic power control on selected TMs transacted by the β metric.

In order to compare independent interfaces with different multipath sensitivity levels as well as different radio frequency carriers and power regulation rules, the α metric of the GLB metric computes *normalized* link budget parameters with respect to idealistic cases given by additive white Gaussian noise (AWGN) performance at the PHY layer and free space path-loss connected to a perfect propagation link. The multipath power sensitivity $S_{M,}$ expressed in decibel-milliwatts (dBm), is the minimum

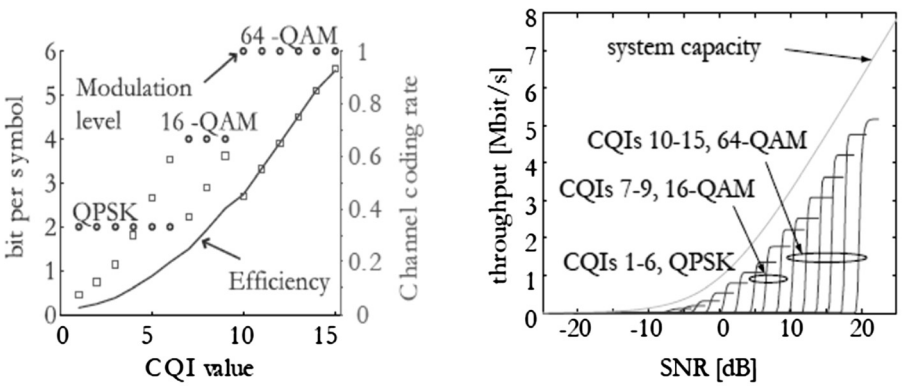

Fig. 2 CQI value and modulation level correspondence, from [18]

required received power at the PHY layer of a given TM which guaranties the QoS settled by a maximum BLER or bit error rate (BER) on data transmission.

The GLB metric differs from the SE link adaptation processing in working with a throughput range fixed by the concerned service instead of the highest possible throughput as performed by AMC processing (Section 2). It is the first element arguing on PE oriented radio link selection. Furthermore, the proposed procedure to estimate the metric detailed in Section 3.2, differentiates the line of sight (LOS) and obstructed and non-line of sight (OLOS/NLOS) propagation links, improving the selection with a conceivable transmit power reduction. The next subsection details the meaning and the mathematical description of the $\{\alpha,\beta\}$ metric.

3.1 The GLB metric model

The α-metric evaluates, for each TM in a dedicated deployment scenario, two relative degradation parameters, the multipath channel margin (MCM) derived from the PHY/MAC layer link level performance and the path-loss margin (PLM) deduced from the path-loss propagation signature characterized by obstacles obstructing the Fresnel zone. MCM expressed in decibels, provides, for a given TM, the exceeded SNR which is compulsory to generate the same BER/BLER as in AWGN. MCM may be alternatively estimated in either considering the difference between the multipath power sensitivity S_{M} and the AWGN power sensitivity S_{AWGN} or the required SNR difference between the multipath and idealistic case ($\mathrm{SNR}_{\mathrm{AWGN}}$) as expressed below:

$$\begin{aligned}
&\mathrm{MCM} = S_{\mathrm{M}} - S_{\mathrm{AWGN}} = \mathrm{SNR} - \mathrm{SNR}_{\mathrm{AWGN}} \quad (\mathrm{dB})\\
&S_{\mathrm{AWGN}} = \mathrm{SNR}_{\mathrm{AWGN}} + \underbrace{10\cdot\mathrm{Log}(kTB_w)}_{P_N} + L_0 \quad (\mathrm{dBm})\\
&S_{\mathrm{M}} = \mathrm{SNR} + \underbrace{10\cdot\mathrm{Log}(kTB_w)}_{P_N} + L_0 \quad (\mathrm{dBm})\\
&S_{\mathrm{ref}} = 10\cdot\mathrm{Log}(kT_{\mathrm{ref}}B_{\mathrm{ref}}) = -114 \quad (\mathrm{dBm}),\\
&\mathrm{NF} = 10\cdot\mathrm{Log}\left(\frac{T}{T_{\mathrm{ref}}}\right), B_{\mathrm{ref}} = 1\mathrm{MHz} \quad (\mathrm{dB})\\
&S_{\mathrm{M}} = \mathrm{SNR} + \mathrm{NF} + S_{\mathrm{ref}} + 10\cdot\mathrm{Log}(B_w) + L_0(\mathrm{dBm})
\end{aligned} \tag{2}$$

As shown in (2), the power sensitivity is calculated from SNR and thermal noise power P_{N}; the amplifier non-linearity's is neglected. The *multipath power sensitivity*, S_{M}, translates the *required power level* to transmit data with a targeted BER associated to a TM delivering a data throughput D, in a multipath context. S_{AWGN} is the power sensitivity under AWGN channel related to the same TM and throughput D. S_{ref} is the thermal noise power with a reference noise temperature set to 290 K, k is the Boltzmann constant, NF is the noise figure affiliated to a noise temperature T, bandwidth (Bw) is the efficient transmission bandwidth, and Lo describes various wired connectivity losses involved by imperfect hardware connections at the transceiver and receiver sides.

Figure 3 illustrates the MCM values affiliated to two MCS deduced from link level simulations performed on the IEEE 802.11ac standard [24] in single input single output (SISO) configurations. MCM is deduced from the BER plot versus the SNR associated with MCS and QoS materialized by maximum BLER thresholds fixed by the QoS. The MCM#1 linked to QPSK 5/8 MCS is the difference in dB between the required SNR in multipath (MP-QPSK 5/8 curve on Fig. 3) and AWGN (AWGN-QPSK 5/8 curve on Fig. 3) along QoS#1 in conjunction with a BER set to 10^{-5}. A similar illustration is given with MCM#2 (BER versus SNR plots with blue curve), considering 16-quadrature amplitude modulation (QAM) modulated signals with a forward error coding (FEC) rate set to three fourths (16 QAM 3/4) and a maximum BER adjusted to 10^{-3} (QoS#2 is representative of voice service, Fig. 3).

The path-loss channel margin (PLM) detailed in (5), measures, in dB, the *path-loss excess* involved by obstacles with respect to the free space path-loss without obstruction. PLM varies with the distance d between the transmitter and the receiver, in relation with multipath $\mathrm{PL}_{\mathrm{MFS}}(d,\mathrm{fc})$ and free space path-loss $\mathrm{PL}_{\mathrm{FS}}(d,\mathrm{fc})$ models expressed below:

$$\begin{aligned}
&\mathrm{PL}_{\mathrm{MFS}}(d,\mathrm{fc}) = PL_0(d_0,\mathrm{fc}) + 10n\mathrm{Log}_{10}\left(\frac{d}{d_0}\right) + \sigma\\
&\mathrm{PL}_0(d_0,\mathrm{fc}) \approx \mathrm{PL}_{\mathrm{FS}}(d_0,\mathrm{fc})\\
&\mathrm{PL}_{\mathrm{FS}}(d,\mathrm{fc}) = 20\,\mathrm{Log}_{10}\left(\frac{4\pi}{c}\right) + 20\mathrm{Log}_{10}(\mathrm{fc})\\
&\qquad + 20\cdot\mathrm{Log}_{10}(d).
\end{aligned} \tag{3}$$

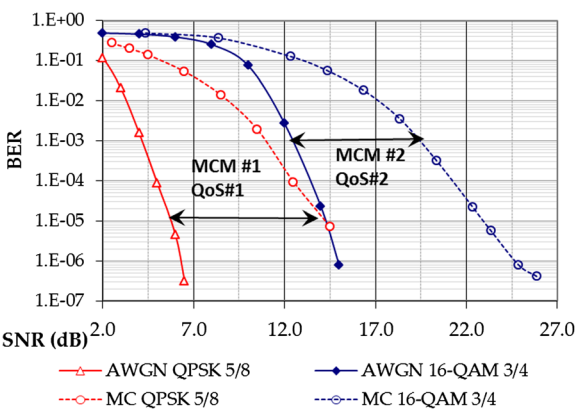

Fig. 3 The multipath channel margin definition

In (3), $PL_0(d_0,fc)$ is a path-loss offset derived from path-loss measurements at a distance d_0 between the transmitter and the receiver in which the attenuation may be assimilated to the free space path-loss when distance d_0 is small. $PL_{FS}(d,fc)$ is the free space path model computed from the Friis equation where c is the speed light, fc is the RF carrier and d is the distance between the transmitter and the receiver. The coefficient n is the exponential coefficient (logarithmic dependency in dB) dependency with the distance d between the transmitter and the receiver and σ is the standard deviation of measurements.

PLM may be either deduced from the path-loss difference between realistic case with obstructions and perfect propagation link, or the available received power difference between multipath, $ARP_{MFS}(d,fc)$, and *idealistic* $ARP_{FS}(d,fc)$ deduced from the free space path-loss. Received power levels are equivalent to the RSSI variations linearly increasing in dB with the EIRP, and depending on receiver antenna gain G_R and path-loss models as detailed in (4):

$$\begin{aligned} ARP_{MFS}(d,fc) &= EIRP + G_R - PL_{MFS}(d,fc) \\ ARP_{MFS}(d,fc) &= EIRP + G_R - PL_{FS}(d_0,fc) - 10n\mathrm{Log}_{10}\left(\frac{d}{d_0}\right) - \sigma \\ ARP_{FS}(d,fc) &= EIRP + G_R - PL_{FS}(d,fc). \end{aligned} \tag{4}$$

The algebraic expression of MCM and PLM are given by

$$\begin{aligned} \alpha &= S_M - S_{AWGN} + \underbrace{PL_{MFS}(d,fc) - PL_{FS}(d,fc)}_{PLM} \\ \alpha &= \underbrace{S_M - S_{AWGN}}_{MCM} + \underbrace{ARP_{FS}(d,fc) - ARP_{MFS}(d,fc)}_{PLM} \end{aligned} \tag{5}$$

PLM variations geared to the distance d, associated to test cases developed in Section 4, are illustrated on Fig. 4. PLM values are derived from path-loss models given in Table 1 at 5 and 60 GHz RF carriers. At 5 GHz, PLM is computed, considering omnidirectional antennas at the transmitter and receiver sides. At 60 GHz, the transmitter azimuth antenna pattern is set to 72° and two different receiver azimuth antenna patterns set to 60° and 10° are selected to increase the radio coverage, limit obstructions, and compensate path-loss offset acquired by the RF carrier. Figure 4 shows that PLM at 5 GHz increases with the distance in both LOS and NLOS because the exponential coefficient n is higher than at 60 GHz due to large antenna pattern (Table 1) translating obstruction occurrence affecting the propagation link. At 60 GHz, the difference between LOS and NLOS situations is highly marked. In LOS, PLM decreases with the distance

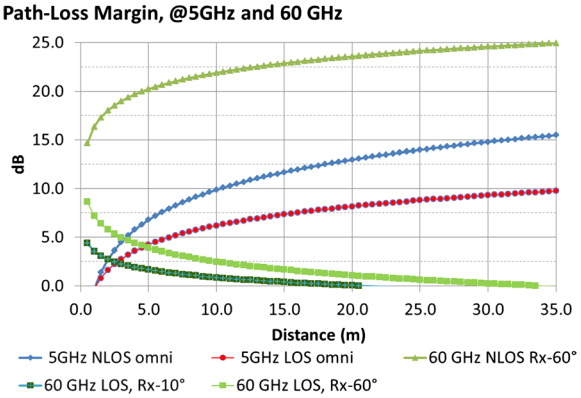

Fig. 4 Path-loss margin at 5 and 60 GHz

meaning that multipath path-loss fast converge toward free space path-loss because of directive antenna use at the transmitter and receiver sides.

The β-metric performs a dynamic power control at the receiver side based on an adjustment between the received power, $ARP_{MFS}(d,fc)$, and the required power S_M of the various candidate TMs resulting from the α-metric decision. Selection is conjunctly finalized with α-metric minimization and β-metric maximization before the power control management resulting in EIRP adjustment by the way of β-metric refinements.

The algebraic expression of the β-metric is given by

$$\begin{aligned} \beta &= ARP_{MFS}(d,fc) + G_R - S_M \\ \beta &= EIRP + G_R - \alpha - S_{AWGN} - PL_{FS}(d,fc) \end{aligned} \tag{6}$$

Figure 5 illustrates the $\{\alpha,\beta\}$ metric principles, derived from the general link budget assessments when considering a single TM denoted "TM1." Radio coverage estimation is obtained when the available received power varying with the distance d converges to the multipath power sensitivity S_M which is a system dependant parameter. Plotted black circles on Fig. 5 give the equality between the available received power and the required power in both realistic and idealistic cases. The figure plots S_{AWGN} and S_M giving the MCM,1 value. In a similar way, the representation of the available received power in realistic and idealistic case (4) allows an estimation of PLM,1 varying with the distance. The β-metric varying with the distance d, is simply calculated with the difference between the available received power $ARP_{MFS}(d,fc)$ and the multipath power sensitivity S_M represented on Fig. 5. The β-metric validity range is restricted to positive values. A power margin (PM) may be added to cover shadowing variations imposing a β-metric minimum threshold higher than PM dB. PM may differ rather we consider LOS or NLOS propagation links.

Table 1 Path-loss models at 5 and 60 GHz

	60 GHz			5 GHz	
	LOS	NLOS	LOS	LOS	NLOS
Tx-Rx, antenna pattern, gains	72°–60°, 10–13 dB		72°–10°, 10–24.8 dB	Omni, 4 dB	
n	1.53	2.56	1.73	2.65	3.03
PL(d_0, fc) (dB)	71.2	79.79	68.01	46.42	46.51
σ (dB)	3.92	5.04	1.6	0	

Figure 6 is in relation with the use case developed in Section 4.1 in which the user equipment may select two different access points (APs) using two different TMs exhibiting S_{M1} and S_{M2} multipath power sensitivity levels to forward the service. On Fig. 6, we assume the AWGN power sensitivity S_{AWGN} is similar for the two TMs. LOS and NLOS propagation conditions differ with the AP1 and AP2, respectively. The GLB $\{\alpha,\beta\}$ metric is evaluated on each TM/air interface (AI) associated to AP1 and AP2, respectively, supplying $\{\alpha_1,\beta_1\}$ and $\{\alpha_2,\beta_2\}$ metric variations. The AP selection is the one giving the lowest degradation, i.e., the minimum α-metric value and the largest β-metric value before transmit power adjustment applied on the selected AP by the α-metric. Distances may be different for these two links.

3.2 Assessment methods of the GLB metric

The proposed method to practically measure the $\{\alpha,\beta\}$ metric, optimize β and refresh the selection, is centered on the MCM and PLM estimations using signaling frames and preamble headers associated to each interface and a LOS/NLOS discrimination thanks to the introduction of original normalized propagation selectivity parameters with respect to system parameters, leading to a refined radio link selection with the GLB metric.

CQI metrics usually use RSSI elements and BLER LUT supplying the correspondence between the BLER and the required SNR to select a MCS in a single AI (Section 2). The assessment method proposed for the GLB metric is similar, in providing, for each AI and TM, evolved LUT with a LOS/NLOS radio link identification, and the use of MCM and PLM outputs to compare independent interfaces. The problem statement is then to identify LOS/NLOS propagation conditions deduced from the channel state information. *Normalized propagation parameters* are then defined, characterizing the link reliability between different TMs and propagation conditions. These *normalized multipath propagation parameters* with respect to PHY system parameters point out on pre-established BER LUT differentiating LOS/NLOS criteria leading to required power levels in relation to BER/BLER targets. It then allows MCM, PLM, and α and β metric calculations upon LOS and NLOS

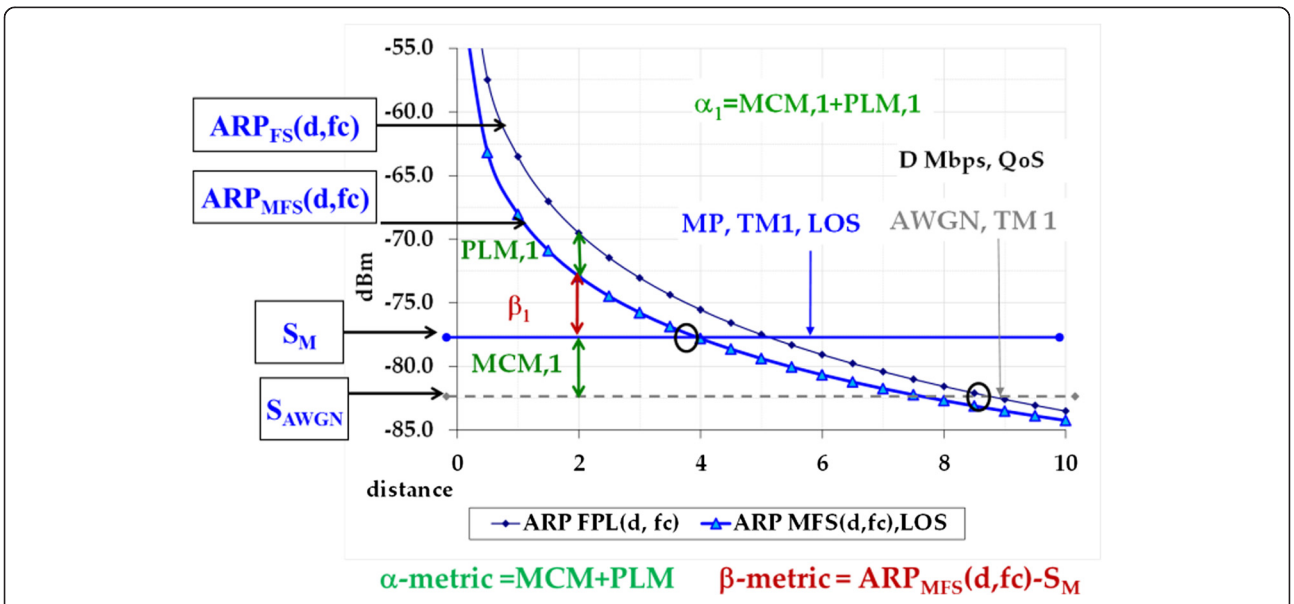

Fig. 5 The $\{\alpha,\beta\}$ metric representation for a single AI/TM

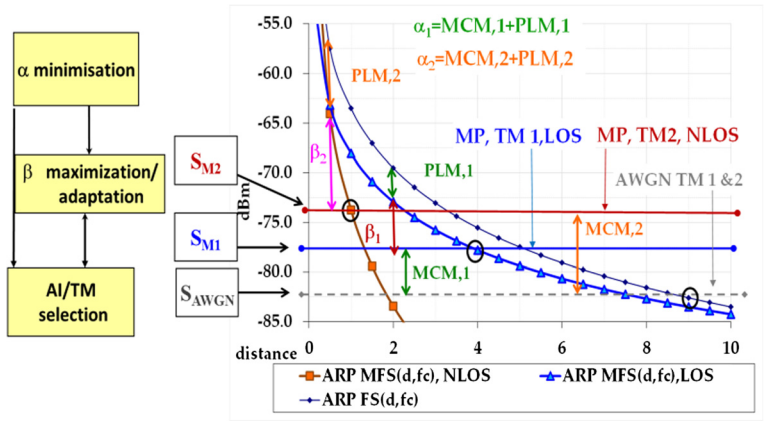

Fig. 6 The {α,β} metric representation with multiple LOS and NLOS links

conditions, respectively. RSSI values may provide elements used to evaluate PLM thanks to available distance information, known as EIRP and antenna characteristics given in PLCP headers of the concerned AI. In addition, the rice factor value deduced from the RSSI power distribution [25], may confirm the radio link obstruction degree. The power sensitivity is usually given in standards and may be registered in dedicated tables. The β-metric estimation may be deduced from α-metric assessments (6). The synoptic of MCM, PLM, and S_M estimation is illustrated on Fig. 7.

Normalized propagation parameters are derived from the equalization processing supplying the multipath channel state information (CSI), typically the equivalent baseband channel impulse response (CIR) of the propagation channel, $h(t,\tau)$, where h(t,ti), ti has to be written with the symbol policy translates time variations of complex amplitude of the channel, over time variant relative delay τi(t) of the CIR (7). The RMS delay spread, the coherence bandwidth with a correlation coefficient set to 0.5 and 0.9 are utilized to design normalized propagation parameters sensitive to LOS/NOS conditions able to point on appropriate BER look-up tables for any PHY layer systems.

The *normalized delay spread diversity order* O_{DS} is expressed in (8) as the ratio of the transmission symbol period T_{SYM} and the RMS delay spread σ_{DS}. The RMS delay spread σ_{DS} supplies the average standard deviation of multipath weighted by power probability γ_I of each delay i. The *frequency diversity order* O_{FD} in (8) is the ratio of the efficient Bw of the PHY system and the coherence bandwidth Δf_y^{cb} of the propagation channel. The coherence bandwidth Δf_y^{cb} is the frequency spacing for positive frequency components, providing a y factor decrease of the normalized average correlation function |RH(Δf)| magnitude of the channel with respect to no frequency deviation (Δf = 0). Δf_y^{cb} is the coherence

$$\alpha = S_M - S_{AWGN} + PL_{MFS}(d,fc) - PL_{FS}(d,fc)$$
$$\alpha = \underbrace{S_M - S_{AWGN}}_{MCM} + \underbrace{ARP_{FS}(d,fc) - ARP_{MFS}(d,fc)}_{PLM}$$

MCM
- ❶ **LOS/NLOS discrimination** using APDP and **normalized selectivity parameters.**
- ○ **Rice factor** based on power distribution within the time window of the frame
- ❷ **Link level** pre-established LUT for each scenario and available AI
- ❸ **SM and S_{AWGN} calculation** with CQI to SNR mapping upon LOS/NLOS/AWGN

PLM
- ❶ RSSI measurements and calculation of the ideal RSSI.
- ❷ LOS/NLOS identification and path-loss model association
- ○ Tx Power known, Antenna gain, distance in PLCP
- ○ Distance deduced from localization techniques

Fig. 7 The assessment procedure of the {α, β} metric and S_M

bandwidth with a correlation coefficient adjusted to y. $P(t)$ is the instantaneous power of the propagation CIR $h(t,\tau)$. These parameters are expressed below

$$
\begin{aligned}
h(t,\tau) &= \sum_{i=1}^{N} h(t,\tau_i)\cdot\delta(\tau-\tau_i(t)) \\
\gamma_i &= E\left\{\frac{|h(t,\tau_i(t)|^2}{P(t)}\right\}, \\
P(t) &= \sum_{i=1}^{N}|h(t,\tau_i)|^2 \\
\sigma_{\mathrm{DS}} &= E\left\{\sqrt{\frac{\sum_{i=1}^{n}\tau_i^2|h(t,\tau_i(t))|^2}{P(t)} - \left(\frac{\sum_{i=1}^{n}\tau_i|h(t,\tau_i(t))|^2}{P(t)}\right)^2}\right\} \\
\mathrm{RH}(\Delta f) &= E\left\{\mathrm{FFT}_{\tau}\left\{\sum_{i=1}^{n}|h(t,\tau_i(t))|)^2\right\}(\Delta f)\right\}
\end{aligned}
\tag{7}
$$

$$
\begin{aligned}
B_{\mathrm{cy}} &= \Delta f_y^{\mathrm{cb}} \Rightarrow \left|\mathrm{RH}\left(\Delta f_y^{\mathrm{cb}}\right)\right| = y\cdot|\mathrm{RH}(\Delta f=0)| \\
O_{DS} &= \frac{T_{\mathrm{SYM}}}{\sigma_{\mathrm{DS}}}, O_{\mathrm{FD}} = \frac{B_w}{\Delta f_y^{\mathrm{cb}}}
\end{aligned}
\tag{8}
$$

An illustration is given in Table 2 in a mixed indoor-outdoor use case. Normalized propagation parameters are evaluated upon the multi-rate filter propagation channel model [26] which resamples and filters the measured propagation channel, adapted to the PHY waveform of the system and simulated use cases. This model is applied at 60 GHz related to the ECMA-368 standard [20] transposed at 60 GHz and at 5 GHz in relation with the IEEE802.11ac/11n system [24]. Representative measurements are used at 60 GHz with a LOS, OLOS, and NLOS discrimination as inputs of the multi-rate filter propagation model. The reference TGac multipath channel model [27] channels D and E have been chosen to differentiate LOS and NLOS multipath signature on the propagation channel models representative of mixed indoor and phantom cell scenarios.

Normalized propagation parameters in the Table 2 highlight different values for LOS and NLOS situations. The O_{DS} decreases and the O_{FD} increases with the obstruction level of the radio link. The O_{FD}-0.5 is almost doubled when passing from LOS to NLOS. The introduced normalized propagation parameters, O_{DS} and O_{FD_y} with y taking two values {0.5, 0.9}, allow a LOS/NLOS discrimination upon independent air interfaces exhibiting different time-related PHY parameters.

As illustrated on Fig. 8, the power distribution within the time window of the frame may also provide a rice factor estimation [25] deduced from the RSSI distribution, leading to LOS/NOS discernment as a complement of the normalized propagation method. Pre-established LUTs of each scenario and available AI (terminal and BS) with LOS/NLOS separation are then used to extract S_{M} values of every considered TM/AI modes.

PLM is deduced from RSSI measurements, equivalent to the available received power $\mathrm{ARP}_{\mathrm{MFS}}(d,\mathrm{fc})$ expressed in (5) and calculations of an ideal RSSI, i.e., $\mathrm{ARP}_{\mathrm{FS}}(d,\mathrm{fc})$, deduced from the free space path-loss model. EIRP, receiver antenna gain G_{R}, and the distance d of the link which is furnished in AI headers.

4 GLB metric performance in multi-RAT scenarios

4.1 Test cases

The GLB metric is evaluated in the context of small-cell hot spot deployment in ultra dense urban and large indoor areas with a distance range up to 40 m. The transmitter and the receiver are able to communicate with

Table 2 Normalized propagation parameters

	Multi-rate filter model [26] 60-GHz ECMA-368 standard			Multi-rate filter model [26] applied to TGn channel models 5-GHz WLAN systems	
	LOS typical	OLOS typical	NLOS atypical	LOS channel D	NLOS channel E
Bw/BT	507/528 MHz			35.63/40 MHz	
T_{SYM} (ns)	312.42			4000	
ODS	132.38	45	26.3	80	40
OFD-0.5	4	8	14	12	24
OFD-0.9	13	54	221	91	91
σ_{DS}	2.36	6.94	11.9	50	100
Bc-0.5	114	62.9	37.2	3.04	1.48
Bc-0.9	39.2	9.3	4	0.39	0.39
d(Tx-Rx) m	8.0	8 .0	12	10-50	10-50

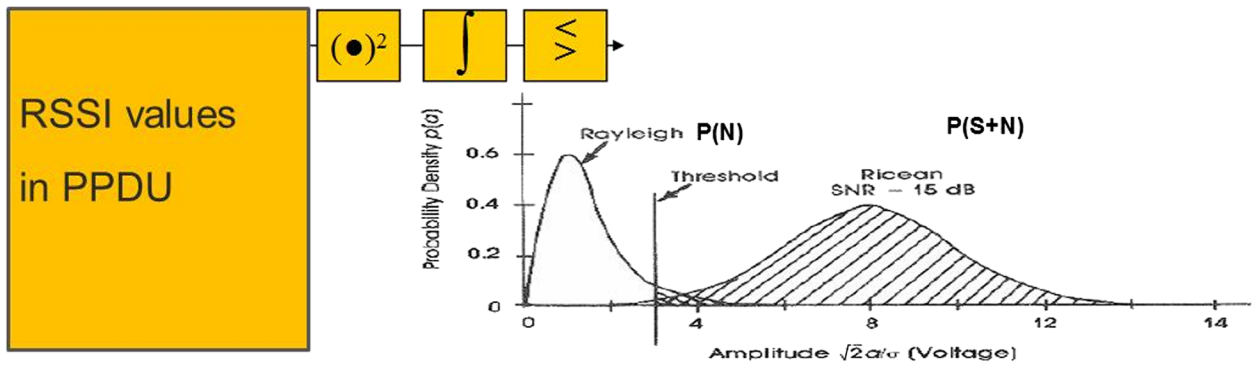

Fig. 8 LOS/NLOS discernment using power distribution [25]

IEEE802.11ac/n [24] and multi-band UWB orthogonal frequency division multiplex (OFDM) interfaces [2, 20] operating, respectively, at 5 and 60 GHz. The first envisioned test case shows benefits of the GLB metric use instead of the SE 3GPP metric using directly RSSI levels to select TMs leading to the largest throughput TM (Section 2). The second test case compares different multiple input multiple output (MIMO) TMs using variable spatial stream number and bandwidth related to a single air interface, the IEEE802.11ac standard [24] and a throughput close to 80 Mbps. The last test case illustrates access point (AP) selection performed by GLB metric to establish a communication with the UE. Furthermore, the radio link propagation reliability varies with considered AP positions.

GLB metric versus SE CQI decision test case is a test case which compares the decision done by the SE maximization criterion as adopted in 3GPP and IEEE802.11n (Section 2) and the decision performed by the GLB metric applied on IEEE802.11 ad standard TMs dedicated to 60-GHz transmissions. For that purpose, we compare $\{\alpha,\beta\}$ metric variations along with different throughputs ranged from 1386 to 4158 Mbps. GLB values are deduced from link level performance carried out in [28]. SE-based decision would choose the highest throughput. The GLB metric performs the TMs selection in targeting throughput requirements and minimum α-metric values. Results are detailed and commented in Section 4.2.

The multiple TM MIMO test case considers a UE equipment connected to a single AP able to deliver and receive different IEEE802.11ac/n MIMO TMs under NLOS conditions delivering a data rate targeted to 80 Mbps. Spatial division multiplex (SDM) MIMO modes are compared together with a variable number of spatial streams, denoted NSS, MCS, and bandwidth size (20 or 40 MHz). Spatial time block coding (STBC) using Alamouti code is integrated in the evaluation. MIMO spatial division multiplexing SDM (NSS, N_{TX}, N_{RX}) represents the usual SDM technique considering N_{STS} time-spatial streams, N_{TX}, and N_{RX} antennas at the transmitter and receiver sides, respectively. STBC (NSS, N_{TX}, N_{RX}) refers to the Alamouti code implementation with a number of spatial stream ($NSS = 1$) lower than the number of time-spatial stream ($N_{STS} = 2$) to perform spatial redundancy processing.

The multi-RAT UE AP selection test case considers a UE connected to two separate AP. One AP, in a OLOS/NLOS propagation link with the UE, delivers two IEEE802.11ac TMs related to SISO and MIMO STBC TM which corresponds to the most outstanding TM selected in the multiple TM MIMO test case. The second AP, in LOS with the UE, generates 60 GHz MB-UWB signals associated with the ECMA-368 standard [20]. GLB metric is applied to perform AP selection combined with TM selection with a throughput ranged to 80 Mbps.

4.2 Performance

IEEE802.11ac [24] and ECMA-368 [20] TM performance are described in Table 3 for large indoor areas and outdoor pico-cell deployments. TM and link level parameters of the IEEE802.11 ad standard are detailed in Table 4. In these two tables, the required SNR values to achieve a BER close to 10^{-5} are deduced from link level performance in connection with the throughput of the TM. SNR values are deduced from BER plot SNRs. The noise figure, NF, used to estimate link budget parameters as detailed in (2) is set to 8 dB at 60 GHz and 10 dB at 5 GHz. Multipath and AWGN power sensitivity values as well as MCM are computed from (2), (3), and (4). MCM values are reported on Tables 3 and 4.

The EIRP associated to the IEEE802.11ac modes operating at 5.25 GHz has been adjusted to 27 dBm and the receiver antenna gain has been set to 4 dB. At 60 GHz, the EIRP is identical, and receiver antenna gains for sectoral and directive antenna are fixed to 13 and 24.8 dB, respectively.

At 5 GHz, new path-loss models differentiating LOS and NLOS links are proposed that are derived from [27] and complementary measurements leading to new path-loss parameters described in Section 3.1 and listed in

Table 3 The IEEE 802.11.ac and 60-GHz ECMA-368 link level parameters

	IEEE802. ac/IEEE802.11n, NLOS				ECMA-368, 60 GHz
MCS_{11n} TM	4	4	26	10	LOS
TM	16-QAM 3/4 *NSS* = 1	16-QAM 3/4 *NSS* = 1	QPSK 3/4 *NSS* = 4	QPSK 3/4, *NSS* = 2	QPSK 1/2
	40 MHz	40 MHz	20 MHz	40 MHz	528 MHz
	SISO	MIMO STBC (1,2,4)	MIMO SDM (4,4,4)	MIMO SDM (2,2,4)	QPSK 1/2
Throughput (Mbps)	81	81	78	81	80
Bw (MHz)	35.63	35.63	17.5	35.63	507.37
SNR (dB)	21.5	16	27.5	20	1.5
NF + L0 (dB)	10 + 2.5	10 + 2.5	10 + 2.5	10 + 2.5	8 + 2.5
S_{AWGN} (dBm)	−71.9	−71.9	−82.05	−78.8	−82.37
S_M (dBm)	−57.94	−64.94	−56.44	−68.44	−77.89
MCM (dB)	13.96	3.96	25.6	10.36	4.48

Table 1. At 60 GHz, measurements have been carried into large indoor areas leading to path-loss parameters differentiating receiver antenna diagram pattern as detailed in the Table 1.

GLB metric performance is discussed upon three test cases described in Section 4.1.

GLB metric versus SE CQI decision test case: IEEE802.11 ad link level performance has been evaluated [28] with a STBC Alamouti code setup in a multiple input single output (MISO) configuration with a single spatial stream (*NSS* = 1), two N_{TX} antennas, and a single receiver antenna N_{RX}. Simulated MCS and associated link level parameters are deduced from simulations (Table 4). GLB metric performance is evaluated upon several MCS delivering different throughput ranges. The SE-based link adaptation processing selects the highest throughput conditioned by the RSSI. GLB metric selection is focused on a throughput targeted by the service, assuming that several TMs may deliver the same throughput. Figure 9 shows that the MCM parameter (2) of the α-metric is sensitive to the FEC rate. MCM estimation may be assimilated α-metric variations with α arbitrary PLM value set in LOS and NLOS for a given distance d. It does not impact conclusions on α-metric variations along with variable throughput ranges. MCM value is lower for the MCS 16QAM 1/2 than for QPSK 3/4 despite a lower throughput delivered by the QPSK 3/4 MCS. This result is reported on both LOS and NLOS and is in favor of SE based AMC processing detailed in Section 2. If we consider the same modulation order, SE-based LA technique would choose the highest code rate and the GLB metric would choose the lowest code rate. Gains resulting from the GLB selection may lead to 1 dB on QPSK modulated signals. The 16 QAM 3/4 and 64 QAM 1/2 MCSs deliver the same throughput. It is interesting to see the MCS selection differ rather than we consider LOS or NLOS. In LOS, the 16-QAM 3/4 MCS is preferred to 64 QAM 1/2 and in NLOS a reverse selection is done. In LOS, lower throughput MCS is selected by the GLB metric decision. These results show the LOS/NLOS discrimination, in the case of LOS/NLOS transitions, is important in the

Table 4 IEEE 802.11.ad OFDM link level parameters

FEC	Forward error coding: LDPC				
MISO (N_{TX}, N_{RX})	MISO (2,1), Alamouti STBC				
$MCS_{IEEE802.11\ ad}$	QPSK 1/2	QPSK 3/4	16-QAM 1/2	16-QAM 3/4	64-QAM 1/2
Data rate (Mbps)	1386	2079	2772	4158	4158
Bw (MHz)	1830.5				
SNR LOS (dB)	3.9	6.7	9.6	13	15
SNR NLOS (dB)	6.5	10.5	12.8	17	18
NF + L0 (dB)	8				
S_{AWGN} (dBm)	−67.57	−64.97	−61.87	−58.57	−56.97
S_M LOS (dBm)	−66.97	−64.17	−61.27	−57.87	−55.87
S_M NLOS (dBm)	−64.37	−60.37	−60.37	−53.87	−52.87
MCM LOS (dB)	0.60	0.80	0.60	0.70	1.10
MCM NLOS (dB)	3.20	4.6	3.80	4.70	4.10

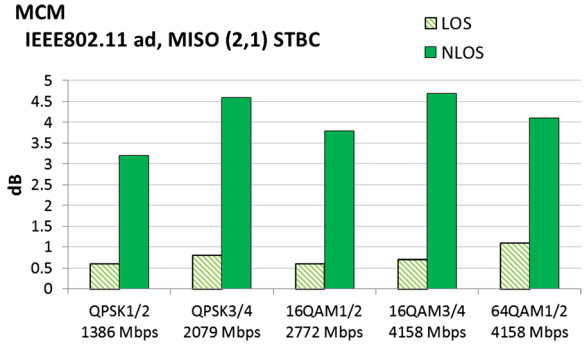

Fig. 9 MCM variations with variable throughput at 60 GHz

MCS selection based on the assessment method proposed in Section 3.2.

The multiple TM MIMO test case compares MIMO spatial stream increase versus transmission bandwidth increase for the IEEE802.11.ac standard combined with two MCS, $MCS_{11n,10}$, and $MCS_{11n,26}$ (Table 3). Two TMs having the same MCS are compared, calculating four spatial streams combined with a 20-MHz bandwidth (SDM (4,4,4), QPSK 3/4) and two spatial streams combined with a 40-MHz (SDM (2,2,4), QPSK 3/4). In addition, a spatial redundancy technique performed by the STBC Alamouti code is compared to MIMO SDM and SISO transmission as detailed in Section 4.1.

Results of Figs. 10 and 11 show that it is more suitable to increase the bandwidth size rather than doubling the number of spatial stream to guarantee QoS and radio coverage and reduce the transmit power level through the β-metric variations. The α-metric gain is then set to 12 dB at a distance of 15 m. The STBC TM using the Alamouti code provides an additional gain set to 2–3 dB with respect to SDM (2,2,4) QPSK 3/4 TM. β-metric variations depicted on Fig. 11 translate quite similar gains as the α-metric. Gains may be translated in a

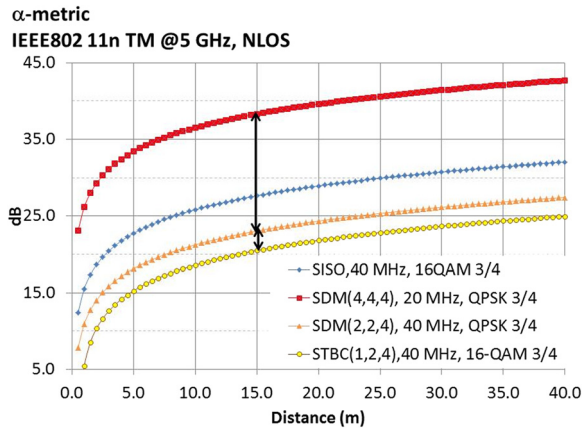

Fig. 10 α-metric variations on IEEE802.11ac TM in NLOS

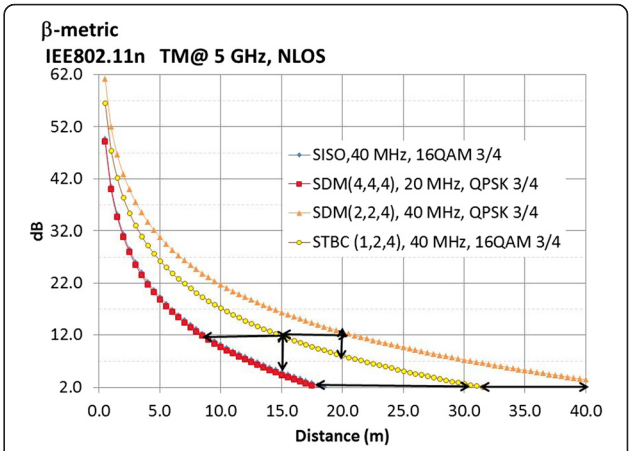

Fig. 11 β-metric variations on IEEE802.11ac TM in NLOS

transmitter power (Tx-power) reduction or a radio coverage extension as illustrated on Fig. 11 and (6). The power reduction given by ΔEIRP is deduced from the β-metric expression as follow:

$$\begin{aligned}\beta &= \mathrm{EIRP} + G_R - \alpha - S_{AWGN} - \mathrm{PL_{FS}}(d, \mathrm{fc}) \\ \Delta\mathrm{EIRP} &= \Delta\beta + \Delta G_R + \Delta\alpha + \Delta S_{AWGN} + \Delta\mathrm{PL_{FS}}(d, \mathrm{fc}).\end{aligned} \tag{9}$$

At a distance d set to 15 m, the power reduction read on the vertical axis may lead 5 dB between $MCS_{11n,10}$ and $MCS_{11n,26}$ modes (Table 3). Keeping constant the Tx-power, the radio extension, read on the x-axis for a β value close to 0, is then doubled. Regarding the β-metric variations, STBC provides lower gain than the SDM (2,2,4) TM following a higher S_M level of the STBC TM as reported on Table 3.

The multi-RAT UE AP selection test case considers one AP, named AP1, delivering an UWB signal associated with the 60-GHz ECMA-368 TM (Table 3) in LOS with two receiver antenna diagrams reported on PLM variations using parameters in Table 1 and results in Fig. 4. The second AP, named AP2, delivers two IEEE802.11ac/n signals over a NLOS propagation link: SISO with a 16-QAM 3/4 MCS and STBC MIMO with a QPSK 3/4 TM are considered with an equivalent efficient bandwidth set to 40 MHz (Table 3).

Results reported on Figs. 12 and 13 show that the 60-GHz transmission is much better than the two IEEE802.11ac TMs when the distance is higher than 2 m, showing that ECMA draws benefits from LOS conditions in the AI/TM selection. α-metric gain leads 14 dB for an identical distance d set to 15 m for the two APs. MIMO STBC TM versus SISO TM highlights gains up to 7 dB at 20 m when considering the MIMO STBC (1,2,4) mode with an identical bandwidth size for these

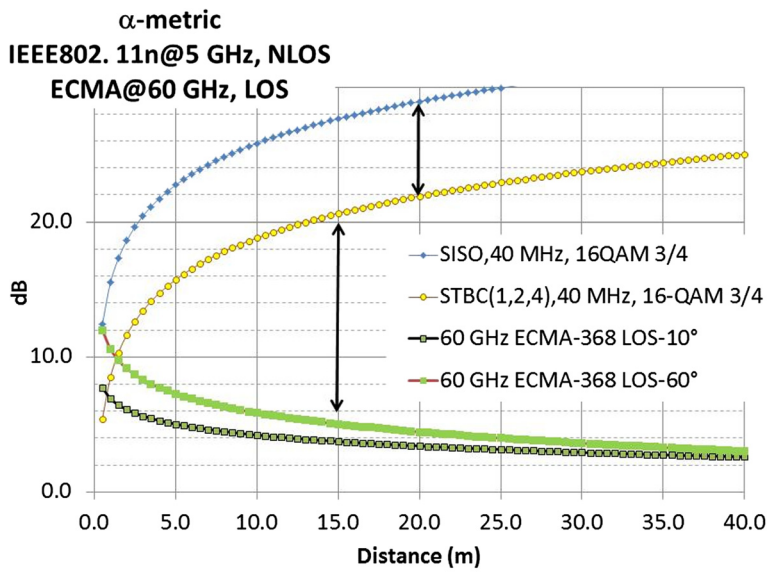

Fig. 12 *α*-metric variations of the multi-RAT UE AP selection test case

two TMs. When comparing with 60 GHz UWB transmissions, additional mm-wave path-loss is compensated by better link level performance resulting from a large transmission bandwidth, taking advantage of multipath combination and LOS propagation link.

β-metric variations, illustrated on Fig. 13, exhibit power gain levels ranged from 10 to 20 dB when selecting a LOS 60-GHz radio link instead of a OLOS 5-GHz transmissions with distance ranging up to 40 m. This gain may be translated in a radio coverage extension when an equivalent Tx-power is set to the two APs. A higher 60-GHz receiver antenna gain, in accordance with Table 1 and (6), is reported on *α*-metric variations following PLM variations depicted on Fig. 4 and directly translated on *β*-metric variations.

5 Conclusions

This paper presents the performance gain of a novel power efficient multi-RAT link adaptation metric, denoted Green Link Budget metric, dedicated to multi-RAT network densification for future 5G networks. In the paper, mm-wave and Wi-Fi technologies for phantom cells with a maximum radio coverage of 40 m are considered. This metric, based on normalized link budget parameters,

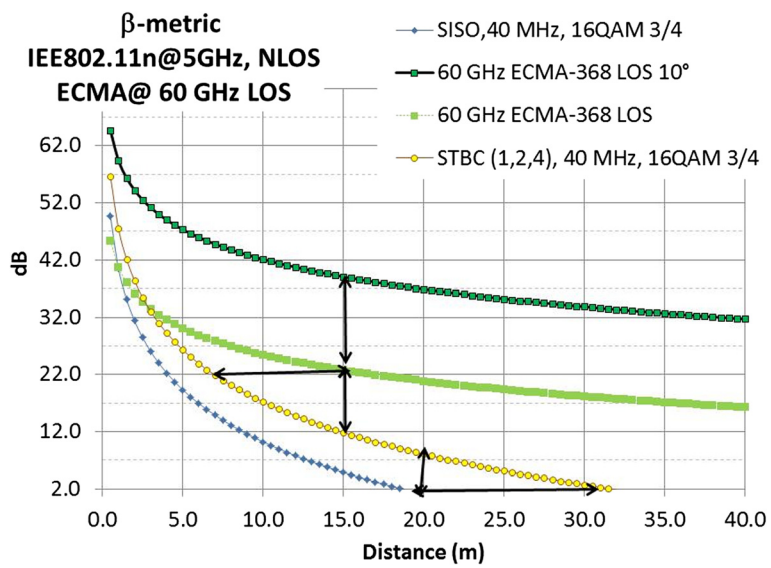

Fig. 13 *β*-metric variations of the multi-RAT UE AP selection test case

allows a fair comparison between independent interfaces and highlights benefits of mm-wave phantom cells with gains ranged from 10 to 25 dB on Tx-power level requirements to guaranty a radio coverage up to 40 m. The next step of the work will be to integrate multi-user distribution in the GLB metric assessments in order to evaluate and optimize multi-RAT end-to-end architectures. The second aspect is to pursue in a multi-user context, the integration of such metrics in emerging C/U plane splitting architectures [10] dedicated WLAN-LTE-A interworking including mm-wave components.

Abbreviations

AI: air interface; AMC: adaptive modulation and coding; ANDSF: access network discovery and selection; AP: access point; AWGN: additive white Gaussian noise; BER: bit error rate; BLER: block error rate; CQI: channel quality indicator; CSI: channel state information; EIRP: emitted isotropic radiated power; FEC: forward error coding; GLB: Green Link Budget; HARQ: hybrid automatic retransmission request; HetNets: heterogeneous networks; LOS: line of sight; LTE-A: Long Term Evolution-Advanced; LUT: look-up table; MCM: multipath channel margin; MCS: modulation and coding scheme; MIMO: multiple input multiple output; MISO: multiple input single output; multi-RAT: multiple radio access techniques; NLOS: non-line of sight; OFDM: orthogonal frequency division multiplex; OLOS: obstructed line of sight; PE: power efficiency; PLM: path-loss margin; PM: power margin; QoS: quality of service; RF: radio frequency; RSSI: received signal strength indicator; SDM: spatial division multiplex; SE: spectrum efficiency; SISO: single input single output; SNR: signal-to-noise ratio; TM: transmission mode; UE: user equipment; UWB: ultra wide-band; WLAN: wireless local area network; MiWEBA: Millimetre Wave Evolution for Backhaul and Access; 3GPP: 3rd Generation Partnership Project.

Competing interests

The authors declare that they have no competing interests.

Acknowledgements

This work has been realized within the framework of the ICT FP7 METIS project (https://www.metis2020.com/) and the STREP EU MiWEBA project (http://www.miweba.eu/#Project) as part of FP7 ICT-2013-EU-Japan supported by FP7 in Europe and MIC in Japan.

Funding

This work was funded with support from the EU FP7 program related to ICT-FP7 MiWEBA project (http://www.miweba.eu) and ICT-FP7 METIS project (https://www.metis2020.com/).

Received: 1 August 2015 Accepted: 13 March 2016
Published online: 01 April 2016

References

1. 5G white paper by the NGMN alliance, Editors : R.E. Hattachi, J. Erfanian, public deliverable, http://www.ngmn.org/fileadmin/ngmn/content/downloads/Technical/2015/NGMN_5G_White_Paper_V1_0.pdf, NGMN 5G Initiative project (2015)
2. I Siaud, AM Ulmer-Moll, Multi-RAT Link Adaptation Techniques for Green Convergent Networks, International Workshop on Cloud Cooperated Heterogeneous Networks, (Osaka, 2013), http://www.mobile.ee.titech.ac.jp/cc-hetnet2013.html
3. ICT 317669-METIS project, Proposed Solutions for New Radio Access, D2.4 METIS Public Deliverable (2015)
4. ICT 317669-METIS project, Final Report on Network-Level Solutions, D4.3 Public Deliverable (2015)
5. ICT FP7 MiWEBA project no 608637, Public Deliverable D1.1, Definition of scenarios and use cases, Editors : I. Siaud, A.M Ulmer-Moll (2013)
6. ICT FP7 MiWEBA project no 608637, Deliverable D1.2, Specification of architecture, Editor : T. Sakurai (2014)
7. RJ Weiler, M Peter, W Keusgen, EC Strinati, AD Domenico, I Filippini, A Capone, I Siaud, A Ulmer-Moll, A Maltsev, T Haustein, K Sakaguchi, Enabling 5G backhaul and access with millimeter-waves, in Proc. EuCNC 2014, Bologna Italy (2014)
8. ICT FP7 MiWEBA project no 608637, Deliverable D3.1, C/U plane splitting, Editor : A. Capone (2014)
9. H Peng, T Yamamoto, Y Suegara, LTE/WiGig RAN-level interworking architecture for 5G millimeter-wave heterogeneous networks. IEICE Trans. Commun. **E98-B**(10), 1957–1968 (2015)
10. I Siaud, AM Ulmer-Moll, H Peng and all, C/U-plane splitting architectures and Inter-RAT management for Radio Reconfigurable Systems, ETSI workshop on Future Radio Technologies focusing on Air Interfaces, Sophia-Antipolis (2016)
11. RP-150510, LTE-WLAN radio level integration and interworking enhancement, 3GPP RAN2 Rel-13 WI, 2015
12. GreenTouch White Paper, GreenTouch Green Meter Research Study: reducing the net energy consumption in communications networks by up to 90 % by 2020, http://docplayer.net/12275541-Greentouch-green-meterresearch-study-reducing-the-net-energy-consumption-in-communicationsnetworks-by-up-to-90-by-2020.html (2013)
13. S Landstrom, A Furuskar, K Johansson, L Falconetti, F Kronestedt, Heterogeneous networks: increasing cellular capacity, Ericsson Review, no. 1, 4-9 (2011)
14. P Vinoth, P Jayakumar, A survey on modulation schemes used for link adaptation in WiMAX networks, Int. J. Comput. Appl. (0975 – 8887) **73**(4), 18-23 (2013)
15. V Tran Sang, MA Eltawil, Link adaptation for wireless systems, Wirel. Commun. Mob. Com. **14**, 1509-1521 (2014)
16. CA Ariyaratne, Link Adaptation Improvements for Long Term Evolution (LTE), Master thesis of Blekinge Institute of Technology (2009)
17. 3GPP, TS 136 213, LTE; Evolved Universal Terrestrial Radio Access (E-UTRA); (Physical layer procedures), V12.3.0 (2014)
18. M Pelcat et al., Physical layer multi-core prototyping, book, Lecture Notes in Electrical Engineering 171, © Springer-Verlag London (2013)
19. MI Salman, CK Ng et al., CQI-MCS Mapping for Green LTE Downlink Transmission. Proceedings of the APAN Network Research Workshop (2013)
20. Standard ECMA-368, High Rate Ultra Wideband PHY and MAC Standard, 3rd edn (2008)
21. 3GPP, TS 23.402, Architecture enhancements for non-3GPP accesses (Release 13), V13.4.0 (2015)
22. MT Kawser, NI Bin Hamid, and all, Downlink SNR to CQI mapping for different multiple antenna techniques in LTE. Int J Inf Electron Eng. **2**(5) 757-760 (2012)
23. 3GPP, TR 36.912, Feasibility study for further advancements for E-UTRA (LTE-Advanced)
24. IEEE Computer Society, Wireless LAN medium access control (MAC) and physical layer (PHY) specifications, IEEE Std 802.11-2012 (2012)
25. J Lansford, Detect and avoid for UWB implementation issues and challenges, In 18th IEEE Internation Symposium on PIMRC (2007)
26. RJ Weiler, M Peter, W Keusgen [HHI], A Maltsev, I Karls, A Pudeyev, I Bolotin [Intel], I Siaud, AM Ulmer-Moll [Orange], Quasi-deterministic millimeter-wave channel models for access and backhaul in MiWEBA. EURASIP Journal on Wireless Communications and Networking-Special Issue on Evolution of Radio Access Network Technologies towards 5G (2016)
27. V Erceg. et al. TGn channel models. Doc. IEEE802.11-03/940r4 (2003)
28. MA Bouzigues, I Siaud, AM Ulmer-Moll, M Hélard, 'Time Reversal and Equal Gain Transmission for 60 GHz millimeter waves Orthogonal Frequency-Division Multiplexing systems', IEEE online conference on green communications (GreenComm), (2014)